frontiers | Frontiers in Immunology

TYPE Original Research
PUBLISHED 09 August 2023
DOI 10.3389/fimmu.2023.1255316

OPEN ACCESS

EDITED BY
Takashi Karako,
National Center For Global Health and Medicine, Japan

REVIEWED BY
Di Xie,
Shanghai Jiao Tong University, China
Yanli Ma,
Shanghai Fourth People's Hospital, China

*CORRESPONDENCE
Jun Ma
mj_xj@sina.cn
Mintao Mao
c3758f@163.com

†These authors have contributed equally to this work and share first authorship

‡These authors have contributed equally to this work

RECEIVED 08 July 2023
ACCEPTED 20 July 2023
PUBLISHED 09 August 2023

CITATION
Wang S, Shi Y, Zhang Y, Yuan F, Mao M and Ma J (2023) Tregs depletion aggravates activation of astrocytes by modulating IL-10/GXP4 following cerebral infarction. *Front. Immunol.* 14:1255316. doi: 10.3389/fimmu.2023.1255316

RETRACTED: Tregs depletion aggravates activation of astrocytes by modulating IL-10/GXP4 following cerebral infarction

Shuai Wang[1†], Yubin Shi[1†], Yanqi Zhang[2], Fengyun Yuan[1], Mintao Mao[1*‡] and Jun Ma[1*‡]

[1]Emergency Department, Tongren Hospital, Shanghai Jiaotong University School of Medicine, Shanghai, China, [2]General Medical Department, Tongren Hospital, Shanghai Jiaotong University School of Medicine, Shanghai, China

Background: Tregs plays a critical role in the development of secondary injuries in diseases. Accumulating evidence suggests an association between ischemic stroke and renal dysfunction; however, the underlying mechanisms remain unclear. This study aimed to investigate the potential of Tregs in inhibiting the activation of astrocytes after focal cerebral infarction.

Methods: This study aimed to investigate the renal consequences of focal cerebral ischemia by subjecting a mouse model to transient middle cerebral artery occlusion (tMCAO). Subsequently, we assessed renal fibrosis, renal ferroptosis, Treg infiltration, astrocyte activation, as well as the expression levels of active GPX4, FSP1, IL-10, IL-6, and IL-2 after a 2-week period.

Results: In the tMCAO mouse model, depletion of tregs protected against activation of astrocyte and significantly decreased FSP1, IL-6, IL-2, and NLRP3 expression levels, while partially reversing the changes in Tregs. Mechanistically, tregs depletion attenuates renal fibrosis by modulating IL-10/GPX4 following cerebral infarction.

Conclusion: Tregs depletion attenuates renal fibrosis by modulating IL-10/GPX4 following cerebral infarction.

KEYWORDS

cerebral infarction, tregs, astrocytes, ferroptosis, IL-10

1 Introduction

Regulatory T cells (Tregs) are present in lymphoid tissues and inflamed areas. However, recent studies indicate that Tregs can accumulate in various non-lymphoid tissues (1). These tissue-specific Tregs recognize self-antigens that are unique to each tissue and possess. The analysis of tissue-specific Treg gene expression in different organs has unveiled distinct phenotypes when compared to Tregs in lymphoid tissues. Tissue Tregs commonly exhibit higher expression of genes like IL-10 and Irf4, along with lower expression of Bcl2, when compared to lymphoid Tregs (2).

The unique characteristics of tissue-specific Tregs may be influenced by the local microenvironment. Tregs develop their characteristics progressively within associated nodes before in their respective tissues (3, 4). In stroke research accumulation of tregs during the two weeks has been observed (5, 6). Brain Tregs contribute to neurological symptom recovery by suppressing excessive activation of astrocytes, a condition known as astrogliosis, through the secretion of Areg (7). Another recent study has demonstrated that osteopontin derived from Treg cells functions through integrin receptors in microglia to boost microglial repair activity (8). The administration of IL-2 after stroke has been found to improve the status of white matter and restore long-term neurological function, supporting the potential therapeutic value of Tregs for neural recovery after stroke (9).

Ferroptosis is a unique form of programmed cell death that is dependent on iron (10). It is characterized by iron accumulation, lipid peroxidation, excessive production of reactive oxygen species, and mitochondrial shrinkage (11). This mode of cell death has a significant impact on the development of numerous complex diseases, including cancer, Parkinson's disease, and sepsis. Due to its critical role in various diseases, ferroptosis has emerged as a focal point of research, with efforts concentrated on identifying small molecules and drugs that can disrupt the process.

Despite considerable advancements in studying tissue-specific Tregs, the molecular mechanisms responsible for their development remain elusive. This study lays the groundwork for comprehending the developmental mechanisms of brain tregs and explores their potential for cerebral infarction.

2 Materials and methods

2.1 Acquisition of microarray data and processing for DEGs

The transcriptome characteristics of the postmortem parietal cortex were compared between individuals who died from sepsis and non-septic critically ill individuals in the GEO database GSE221379. The complete RNA datasets from the selected samples were downloaded for subsequent analysis; however, information regarding the age, etiology, medication treatment, and prognosis of each sample was not available. The raw data was processed using the "Deseq2" R package to identify the differentially expressed genes (DEGs) in the human brain between septic and non-septic critically ill patients.log2 (fold change). The "ggplot2" R package was utilized to create a volcano plot, which illustrates the results. Furthermore, the "pheatmap" R package was employed to perform a bidirectional hierarchical clustering analysis of the collected DEGs (Xiantao tool, www.xiantao.com) (12).

2.2 Gene set enrichment analysis, gene ontology enrichment, and Kyoto Encyclopedia Of Genes And Genomes pathway analysis were performed

To annotate the potential functions of the EP-DEGs, DAVID Bioinformatics Resources v6.8 was employed for Gene Ontology (GO) mapping and Kyoto Encyclopedia of Genes and Genomes (KEGG) pathway analysis. The biological processes (BP), cellular components (CC), and molecular functions (MF) associated with each DEG were assessed. Additionally, all EP-DEGs were submitted to the DAVID website (version 6.8).The enriched GO terms were visualized using the GOplot package in the R programming language. Additionally, the GO plot package was utilized to analyze the overlap of genes involved in the identified GO terms. Furthermore, the pathways in which the DEGs were involved were predicted and mapped using the KEGG database in conjunction with DAVID (Xiantao tool, www.xiantao.com) (13–15).

2.3 Analysis of protein-protein interactions and identification of hub genes

The STRING database's multi-protein online tool was used to predict PPI networks between two genomes, and Cytoscape 3.6.1 was employed to visualize these networks. To explore the biological processes associated with the gene cluster, the genes in the cluster with the highest score were imported into STRING for further analysis of the protein interaction network (Xiantao tool, www.xiantao.com) (16).

2.4 MCAO induction

Throughout the MCAO procedure, the head temperature was maintained at 36° with the assistance of a heat lamp. After 60 minutes of MCAO, the intraluminal suture was removed to achieve brain reperfusion (17). "In brief, mice were anesthetized using a mixture of isoflurane, oxygen, and air. The right common carotid artery was carefully isolated and ligated with a medical suture. Additionally, the right internal carotid artery and external carotid artery were separated. A ligation was performed at a distance of 1 cm from the internal and external cervical vascular branches, specifically at the site of the external carotid artery. A small incision was made proximal to the heart, near the ligated area of the artery. Through this incision, a nylon monofilament coated with silicone and heat-blunted at its tip was carefully inserted into the right internal carotid artery. Laser Doppler flowmetry was utilized to continuously monitor the blood flow in the right brain artery. The filament was secured when its tip reached the origin of the middle cerebral artery, which was confirmed by a recognizable decrease (~30% of baseline) in cortical blood flow. After 1 hour of occlusion, the filament was removed to allow for reperfusion, and the blood flow was restored to more than 70% of the baseline level. For sham-operated mice, the same surgical procedures were performed, with the exception of filament insertion. Throughout the aforementioned procedures, the mice were maintained on a warming pad. A total of 66 mice were successfully induced with MCAO and included in further experiments. However, 15 mice died within 24 hours following reperfusion and were subsequently excluded from the study". In order to investigate the role of Tregs in MCAO, the experimental groups were divided into four groups: Control group, MCAO group, Tregs Depletion +MCAO (DT+MCAO) group, and DT group.

2.5 Immunofluorescence

Brain tissue sections (20 μm) were hydrated and deparaffinized, and antigen retrieval was performed before blocking with 10% bovine serum albumin for one hour at room temperature. Primary antibodies, including anti-2 (1:100, AiFang Biological, AF14722), anti-IL-10 (1:100, AiFang Biological, AF06580), anti-IL-2(1:100, AiFang Biological, AF02481), anti-IL-6 (1:100, AiFang Biological, AF06790), anti-FSP1 (1:100, AiFang Biological, AF14902), and anti-GPX4 (1:100, AiFang Biological, AF06580), were used to incubate the sections overnight at 4°. In the case of astrocyte cells, the cells were initially washed three times in PBS, fixed in 4% paraformaldehyde for 30 minutes, rinsed again in cold PBS, and then permeabilized for 30 minutes with 0.3% Triton X-100. Following the permeabilization step, the cells were blocked with 10% BSA for 1 hour before incubating with relevant primary and secondary antibodies. Observation under a fluorescence microscope (FV3000, Olympus) followed (18).

2.6 Depletion of tregs

To deplete regulatory T cells (Treg cells), diphtheria toxin (DT) was injected intraperitoneally (ip). At a dosage of 0.05 mg/g of body weight, an injection of the antibody CD25 was administered three days before subjecting the rats to a 60-minute transient middle cerebral artery occlusion (tMCAO). To ensure continuous depletion of Treg cells, this injection was repeated every three days until 14 days after the occurrence of the stroke., as previously described. Delayed injection of DT began 5 days after the tMCAO procedure, and then repeated every 3 days until the animals were sacrificed. To deplete microglia and macrophages, the mice (9-10 weeks old, weighing 25-30 g) were provided with PLX5622 in their diet (Research Diets) at a concentration of 1200 parts per million (PPM) or 1200 mg/kg of chow. This treatment was initiated 7 days before surgery and continued until the end of the experiment (19).

2.7 Model of oxygen and glucose deprivation

We employed a previously-described OGD/R procedure. The specific methodology used in this research study was based on the references provided below (20). In this study, astrocyte cultures were divided into four experimental groups: (1) the normal group; (2) the OGD/R group, where astrocytes were washed three times with PBS and cultured in DMEM (no glucose). The cells were then placed in an incubator with an atmosphere of 0.1% O2, 94.9% N2, and 5% CO2 (hypoxia) for 2 hours. After that, the cells were placed in DMEM and incubated in an atmosphere of 95% air and 5% CO2 for 48 hours; (3) the OGD/R+10μg/ml IL-10 group;,where astrocytes were washed with PBS three times and re-suspended in DMEM (no glucose) supplemented with IL-10 (10μg/mL) during OGD/R injury; (4) the OGD/R+10μg/ml IL-10 + 10μM GPX4-inhibitor group, where astrocytes were washed with PBS three times and re-suspended in DMEM (no glucose) supplemented with GPX4-inhibitor (RSL3 10 μM) during OGD/R injury.

2.8 ELISA

ELISA was performed to validate the expression levels of IL-1β, NLRP3, FTL, and TNF-α in four groups. Tissue homogenate or cell supernatant were determined using commercial ELISA kits (IL-1β: Cat. #AF-02323M2 China; NLRP3: Cat. #AF-02936M2, China; TNF-α: Cat. #AF-02415M2, China; FTL: Cat. #JL31443, China.) according to the manufacturer's instructions

2.9 Co-culture of tregs and astrocytes

Tregs were isolated from the spleen and lymph nodes of mice, as previously described. Tregs and glial cells were co-cultured using the following method. The culture medium was removed from the semi-confluent glial cell culture, and Treg cells (1.0×10^6/well) were then added. The cells were cultured in the presence of 2-mercaptoethanol (×1000 dilution), anti-CD3 antibody (2 μg/mL), anti-CD28 antibody (2 μg/mL), for 3–6 days. Half of the medium was changed every 2 days, and anti-CD3 and anti-CD28 antibodies were added only on the first day. Various cytokines were added at the indicated concentrations described below. To prepare the conditioned medium (CM), semi-confluent astrocytes (2×10^5/well) in 24-well dishes were washed three times using serum-free medium, cultured in DEME medium containing 10% FCS supplemented with 4 mM L-glutamine for 24 h, collected in sterile tubes, and stored at −25°C until further use. Subsequently, 0.5 mL of CM was added to the 0.5 mL Treg culture in 24-well dishes.

2.10 Statistical analysis

Statistical analyses were conducted using GraphPad Prism 9.0.The Student's t-test and χ^2 test were used to analyze the normally distributed data, assessing the mean difference between two groups and testing the association between categorical variables, respectively. Non-normally distributed data was analyzed using the Kruskal-Wallis test, a nonparametric test that evaluates differences between three or more groups without assumptions of normality or homogeneity of variance. A significance threshold of $p<0.05$ was set. Normality and homogeneity of variance were tested, and appropriate adjustments for multiple comparisons were made using Bonferroni correction (21).

3 Results

3.1 Processing of sample information and identification of DEGs

The preprocessing of the sample information primarily involves filtering and quality control procedures. The filtering process includes

10.3389/fimmu.2023.1255316

removing low-quality samples and eliminating outliers. Common metrics, such as sequencing depth and ribosomal RNA contamination, are assessed to perform quality control of the samples. Additionally, sample normalization is conducted to ensure the comparability of gene expression levels. The identification of DEGs is achieved through statistical analysis methods, such as the t-test or the DESeq2 package in R.Genes exhibiting significant differences in expression levels, based on specific criteria such as fold change and statistical significance, are classified as differentially expressed genes (DEGs).Subsequent downstream analysis involves further examination and prioritization of these DEGs. This identification process helps to identify key genes that are relevant to the research question of interest. The identified DEGs serve as potential targets for subsequent investigation and functional annotation (Figures 1A–D).

3.2 Functional and pathway enrichment analysis were performed on the differentially expressed genes

In order to gain a thorough understanding of the role of the 31 differentially expressed genes (DEGs) identified in the brain tissue dataset, functional and pathway enrichment analyses were conducted using DAVID. As depicted in Figure 2A, these genes exhibit significant enrichment in biological processes such as zinc ion binding, calcium-dependent protein binding, and cytokine activity. Additionally, they are found to be primarily enriched in the inflammatory response, innate immune response, and neutrophil chemotaxis. The enrichment analysis also revealed that all of these genes are enriched in the extracellular space. Furthermore, they are enriched in various KEGG pathways, using the cnetplot function in

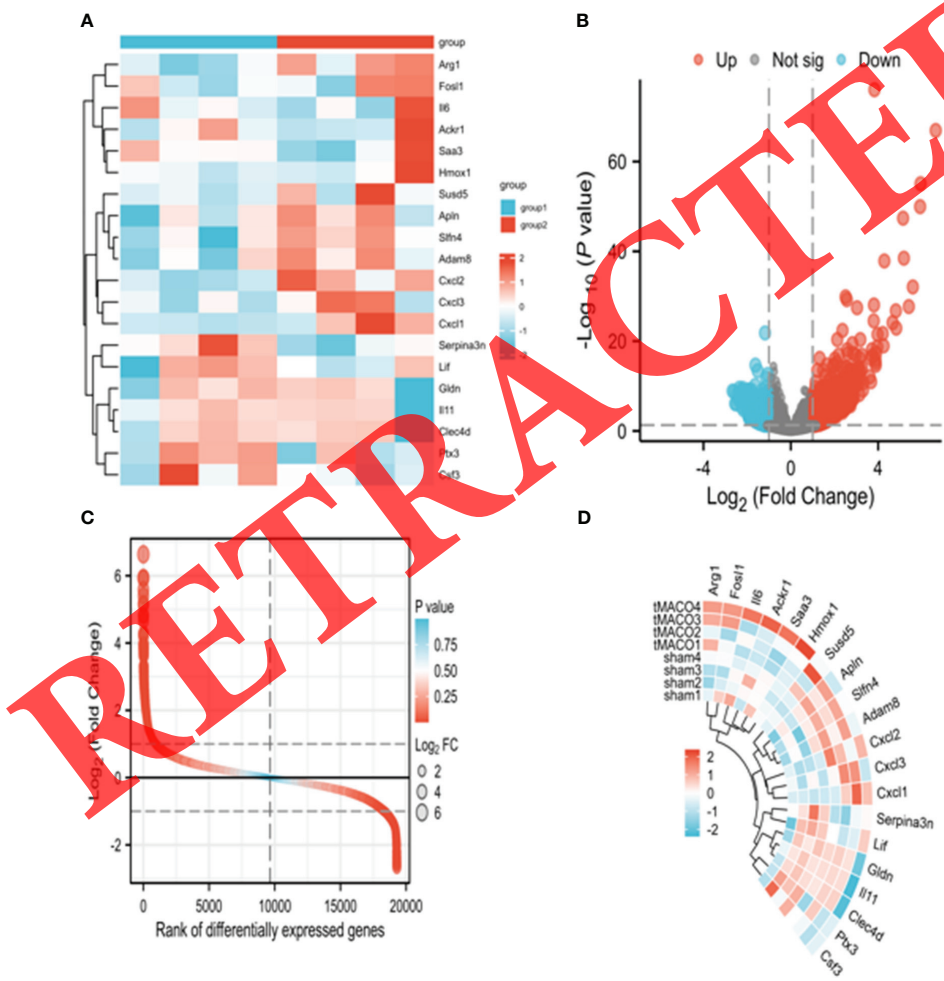

FIGURE 1
Illustrates the data processing and identification of differentially expressed genes (DEGs) .**(A)** presents a boxplot showing the expression levels of gene probes across samples. The median, higher quartile, and lower quartile did not exhibit significant differences. Next, **(B)** depicts a heatmap illustrating the sample-to-sample correlation. The MCAO group displayed a stronger intra-group correlation compared to the control group. **(C)** displays a volcano map generated using the limma R tool, showcasing all the DEGs in both the control and sepsis groups. The map highlights the top 8 up- and down-regulated genes with the lowest p-values. Finally, **(D)** exhibits a heatmap presenting all the DEGs in both the MCAO and control groups.

the ClusterProfiler package. Notably, IL6 and CXCL3,were found to be enriched in at least two BPs, CCs, and MFs (Figures 2A–G).

3.3 We performed gene cluster identification and protein-protein interaction network analysis in this study

Through the application of LogFC in conjunction with KEGG analysis, it was discovered that IL-6 remained involved in the aforementioned processes. To investigate the interactions among the 26 DEGs, we constructed a protein-protein interaction (PPI) network using the STRING database. The PPI network was visualized using the Cytoscape application (Figure 3A).The PPI network consisted of 26 nodes, representing molecular pathways and processes associated with the 26 core DEGs. Working modules were developed using the MCODE plugin for Cytoscape. The results revealed a module consisting of 9 genes (Figures 3B–E).

3.4 Tregs depletion promoted activation of astrocytes of mice with MCAO

To evaluate the potential impact of Tregs in MCAO mice, we conducted an immunofluorescence assay to measure the

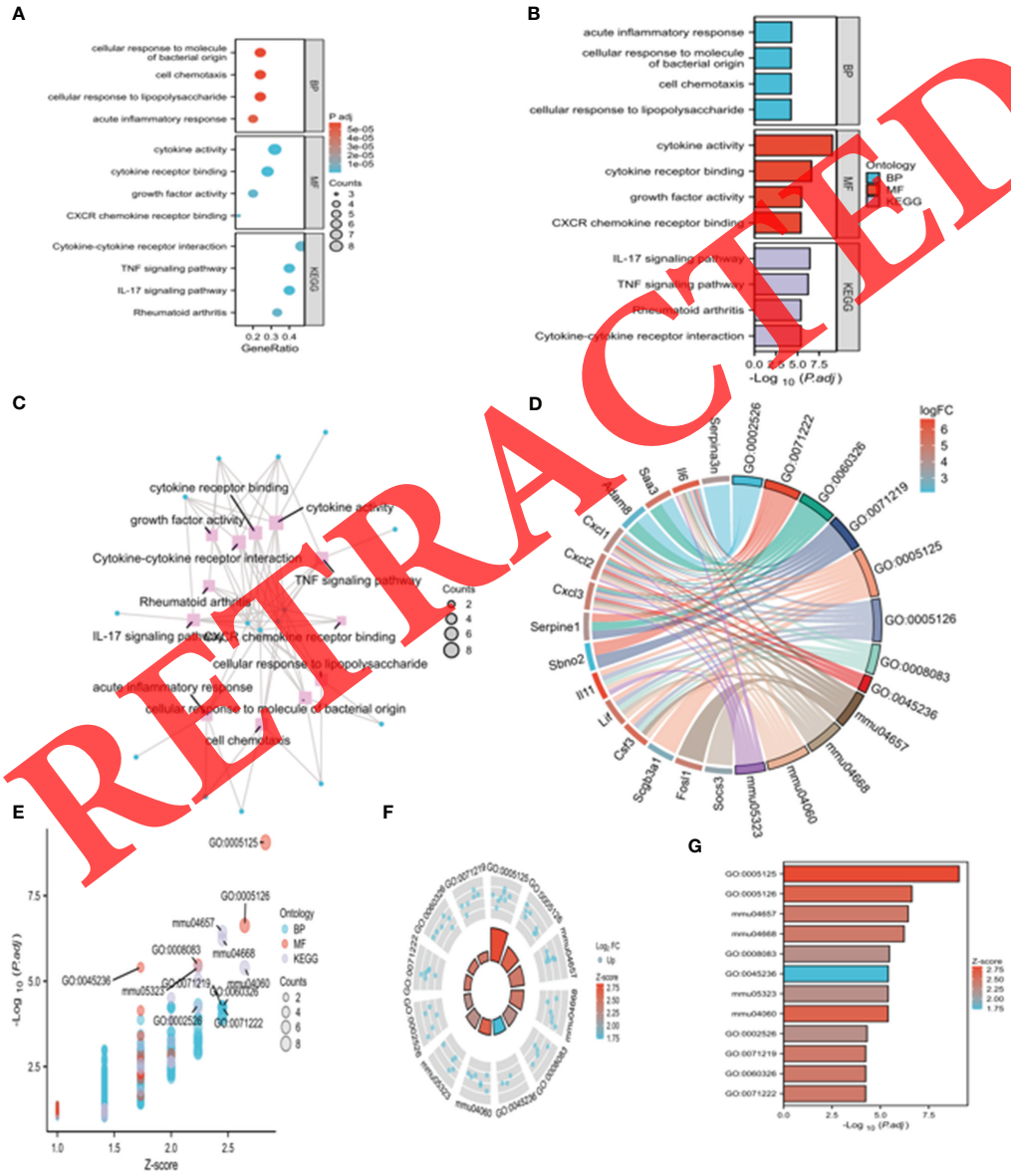

FIGURE 2
presents the Gene Ontology (GO) and Kyoto Encyclopedia of Genes and Genomes (KEGG) enrichment analysis of the differentially expressed genes (DEGs) in the study. In **(A)**, dotplots display the top five enriched GO terms for biological processes (BPs), cellular components (CCs), and molecular functions (MFs). Additionally, five enriched KEGG processes are showcased. **(B–G)** illustrates a circle graph representing the GO enrichment of the DEGs. The circle graph highlights the top five GO categories for BPs, CCs, and MFs, respectively, in which the DEGs are enriched. The colored points within the graph represent the GO categories, with the size of each point indicating the number of genes associated with it. The corresponding category of each point is denoted by the color of the line in the legend.

10.3389/fimmu.2023.1255316

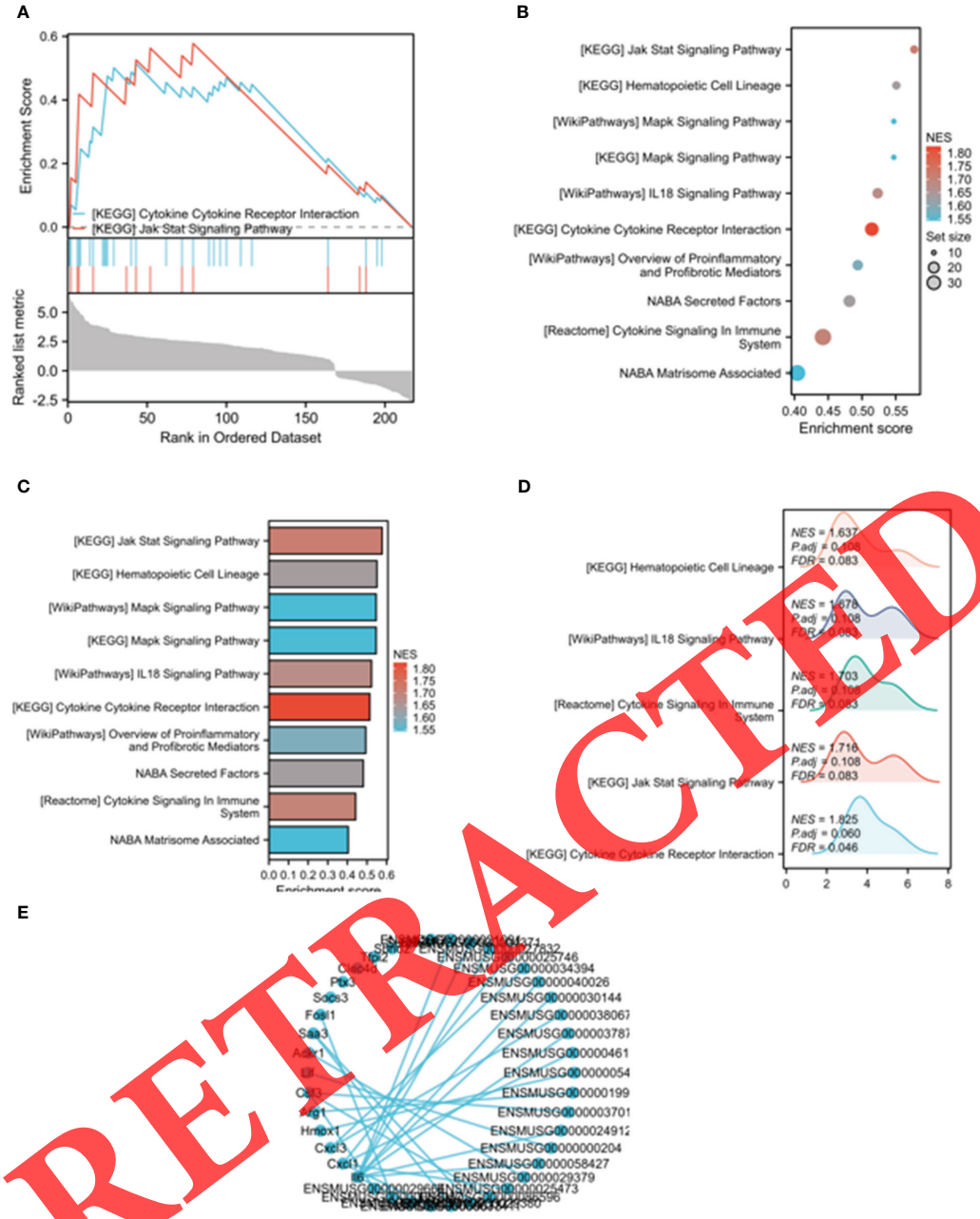

FIGURE 3
Gene cluster identification and protein-protein interaction (PPI) network analysis in this study. Through the application of LogFC in conjunction with KEGG analysis, it was discovered that IL-6 remained involved in the aforementioned processes. To investigate the interactions among the 26 DEGs, we constructed a protein-protein interaction (PPI) network using the STRING database. The PPI network was visualized using the Cytoscape application **(A)**.The PPI network consisted of 26 nodes, representing molecular pathways and processes associated with the 26 core DEGs. Working modules were developed using the MCODE plugin for Cytoscape. The results revealed a module consisting of 9 genes **(B–E)**.

protein expression of two activation of astrocytes markers (IL-2, IL-6) in the brain tissues of each group. Immunofluorescence examination revealed a significant induction in the expressions of IL-2 and IL-6 in the brain of MCAO mice when compared to the control group, which was then promoted in the MCAO +DT group, as demonstrated in Figures 4A–Z. We also examined the expression of inflammatory factors IL-1β, NLRP3, and TNF-α and found that DT could reduce the elevated levels of inflammatory factors caused by MCAO, please refer to supple Figure 4 for the results.

10.3389/fimmu.2023.1255316

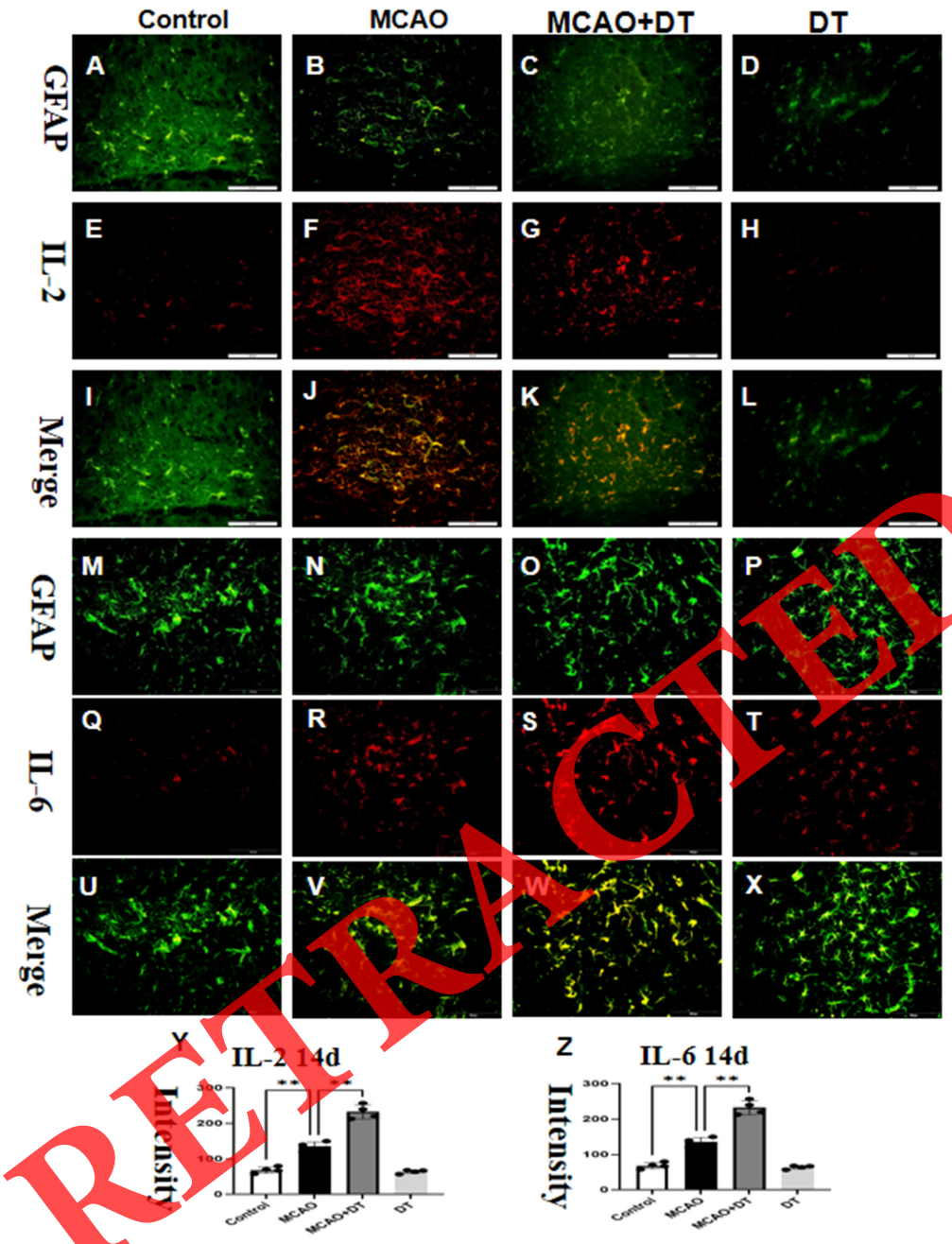

FIGURE 4
Tregs depletion promoted activation of astrocytes of mice with MCAO. Immunofluorescence was used to show the distribution of IL-2 (red, **E–H**) and GFAP (green, **A–D**). The co localization images of the IL-2 and GFAP are shown in **(I–L)**. **(M–X)** depicted IL-6 level across different groups. Immunofluorescence was used to show distributions of GFAP (green, **M–P**) and IL-6 (red, **Q–T**) **(U–X)** with merge pictures. **(Y, Z)** displayed IL-2 and IL-6 bands. The sample size was N=4 with significance set at **P<0.01. Scale bars for A-X were set at 50 μm.

3.5 Tregs depletion decreased astrocytic autophagy

In MCAO mice, there was a significant increase in the production of LC3 in the astrocytes, as illustrated in Figures 5A–J. The electron microscope results showed that the mitochondria in the experimental group exhibited swelling, disappearance of mitochondrial ridges (Figures 5K, L), and an increase in autophagosomes (Figures 5O, P). However, after applying DT intervention, the mitochondrial swelling could be alleviated and mitochondrial autophagy could be inhibited (Figures 5M, N, Q, R).

3.6 Tregs depletion inhibited the astrocytes of ferroptosis

The MCAO group had significantly increased fluorescence intensity levels of FSP1 and decreased in GXP4 compared to the control group (Figures 6A–L). The MCAO reduction in fluorescence

10.3389/fimmu.2023.1255316

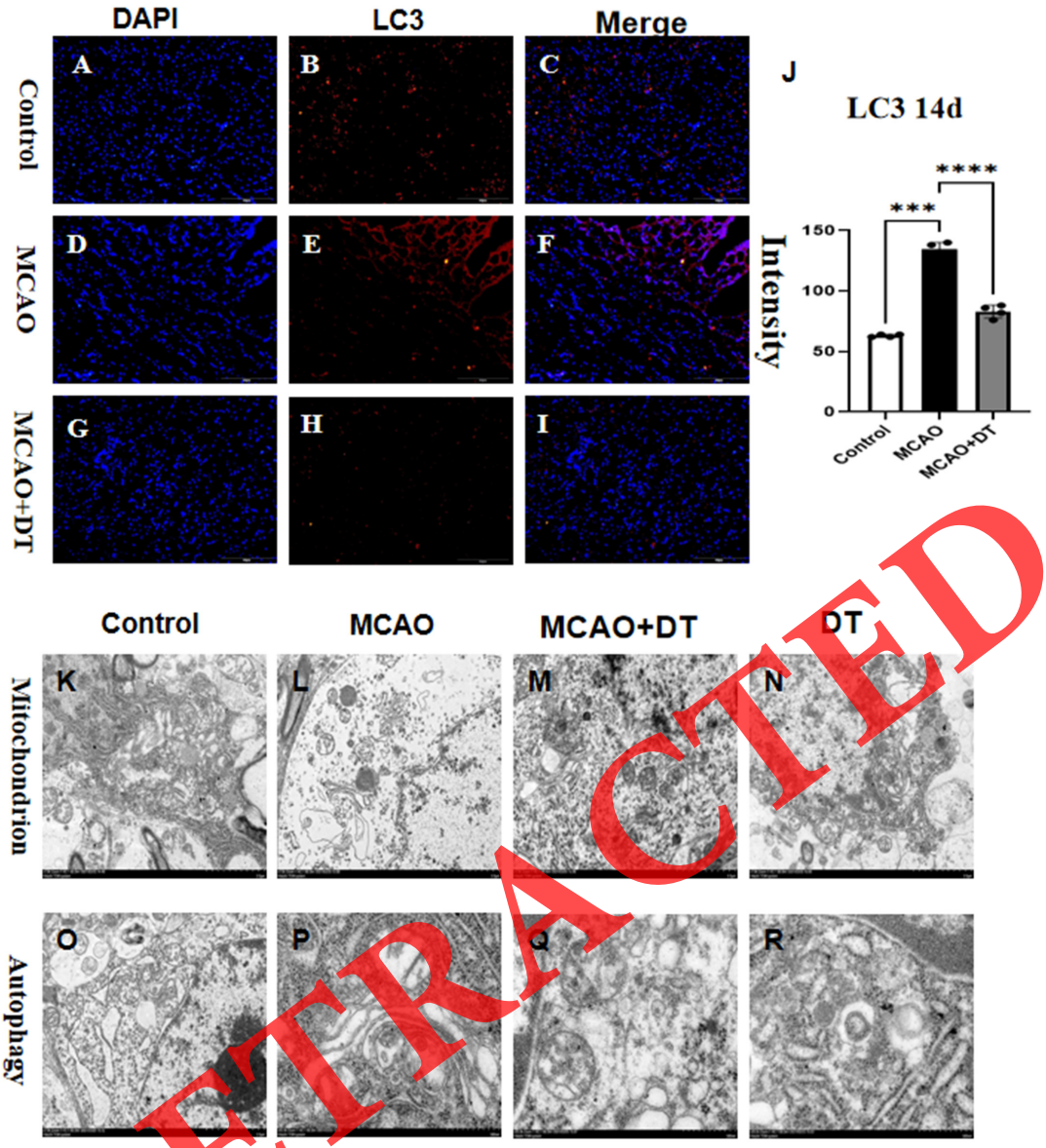

FIGURE 5
Tregs depletion decreased astrocytic autophagy. In order to determine variations in protein expression levels, **(A–J)** depicted LC3 levels across different groups. Immunofluorescence was used to show distributions of LC3 (red, **B, E, H**). Cells are labeled with DAPI (blue, **A–C, G–J**) with merge pictures. Electron microscopy shows changes in autophagosomes consistent with LC3 **(K-N, O-R)**. A sample size of N=4 was used, with significance set at ***P<0.005, and ****P<0.001. Scale bars for A-I were set at 50 μm.

intensity levels of GXP4 and induction in FSP1 was partially attenuated by DT treatment (Figures 6M–Z). We also examined the expression FTL and found that DT could reduce the elevated levels of FTL by MCAO, please refer to supple Figure 6 for the results.

3.7 IL-10 inhibited the expression of IL-6 and IL-2 *in vitro*

In vitro models demonstrated that OGD induces astrocytes activation. Following OGD treatment, the fluorescence intensity levels of IL-2 (Figures 7E–H) and IL-6 (Figures 7Q–T) significantly increased compared to the baseline levels (Figures 7A–D, M–P). The fluorescence intensity levels were comparable in the control group and the OGD+IL-10 group (Figures 7I–L, U–Z).We also examined the expression of inflammatory factors IL-1β, NLRP3, and TNF-α and found that IL-10 could reduce the elevated levels of inflammatory factors caused by OGD, please refer to supple Figure 7 for the results.

38 DT promoted astrocytes ferroptosis by inhibiting the IL-10/GPX4 pathway

In vitro experiments showed that co-culturing tregs with astrocytes (Figures 8A–H) resulted in alleviation of neuroinflammation

10.3389/fimmu.2023.1255316

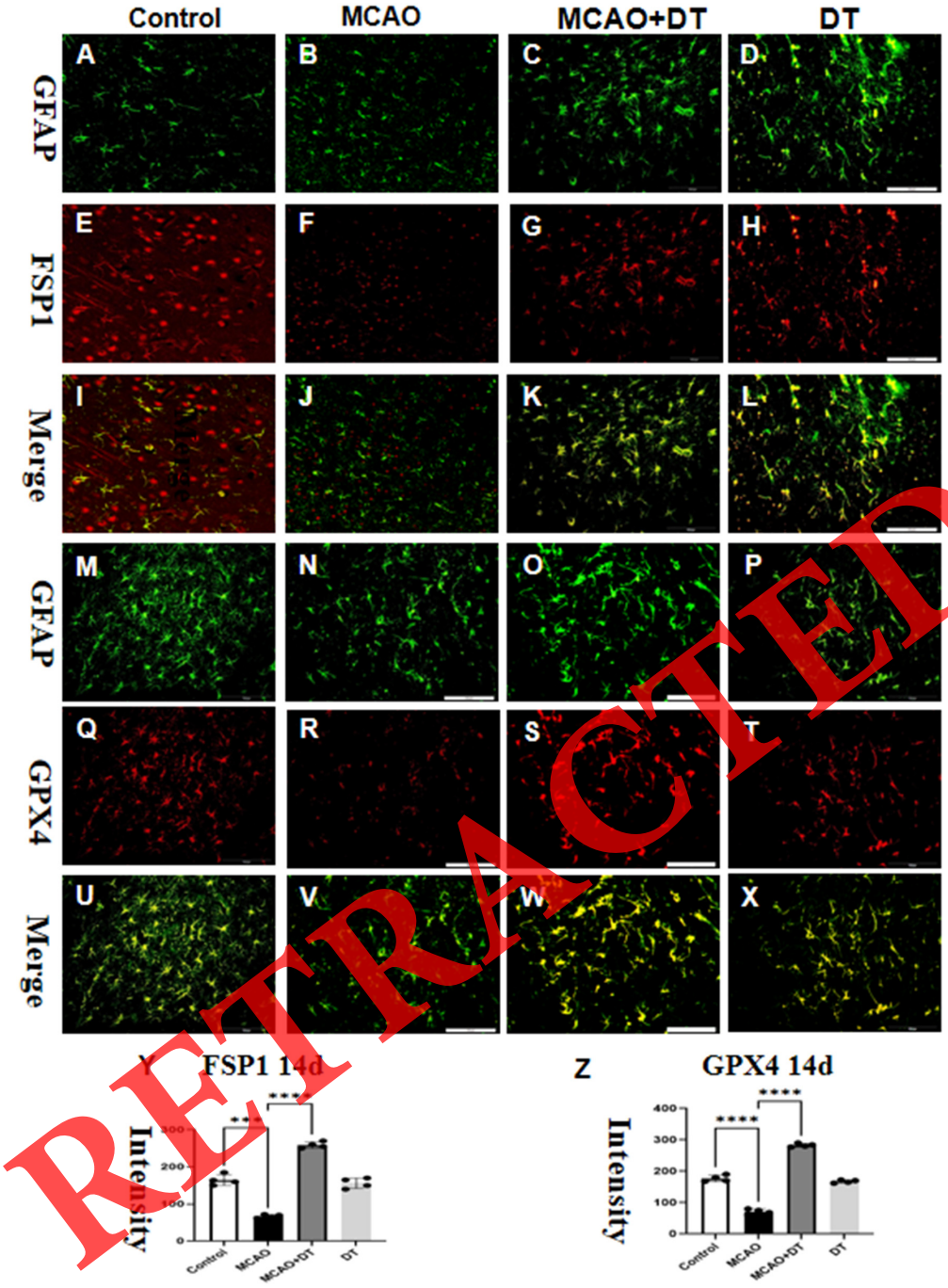

FIGURE 6
Tregs depletion inhibited the astrocytes of ferroptosis. Immunofluorescence was used to show distributions of FSP1 (red, **E–H**) and GFAP (green, **A–D**) with the merge pictures shown in **(I–L)**. Double labeled immunofluorescence showed the expression of GFAP (green, **M–P**) and GPX4 (red, **Q–T**), and the co-localization was shown in **(U–X)**. The flow cytometry image is shown in **(Y)** and **(Z)**, with a sample size of N=4 and significance level of ***P<0.005, and ****P<0.001. Scale bars for **(A–X)** were set at 50 μm.

induced by OGD. Additionally, OGD resulted in a significant decrease in GPX4 protein expression levels (Figure 8J), whereas DT treatment increased GPX4 expression levels in OGD-treated pipes (Figure 8K). Moreover, the addition of IL-10Ra, an IL-10 inhibitor, weakened the effect of OGD (Figure 8L), while clearing tregs *in vitro* weakened the effect of IL-10Ra (Figures 8M–Q).

4 Discussion

The present study investigates how Treg cell-astrocyte interaction creates a microenvironment rich, this intervention aims to tregs during the chronic stages of ischemic stroke. Our data indicate that Treg cells primarily work through the latter

10.3389/fimmu.2023.1255316

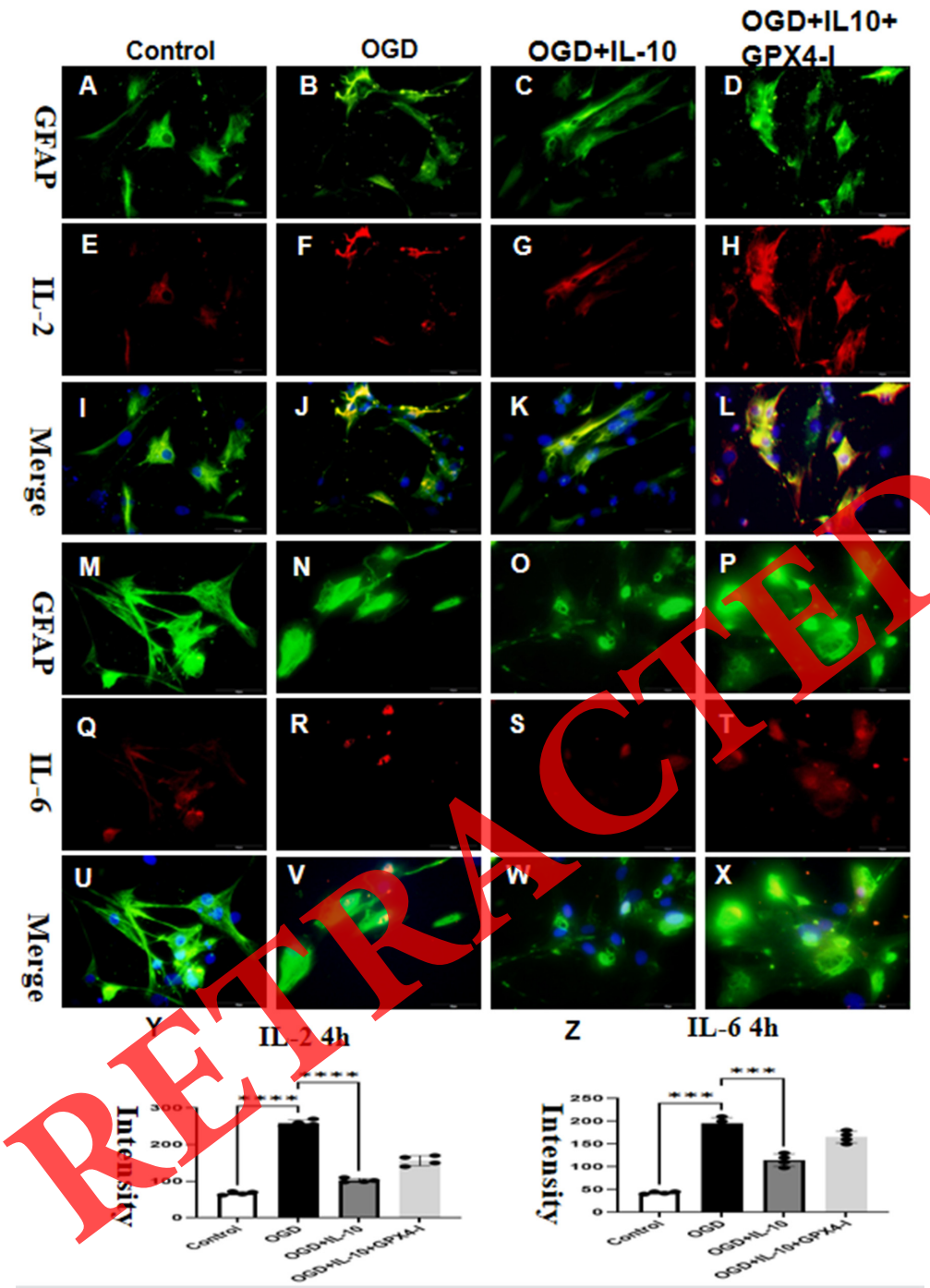

FIGURE 7
IL-10 inhibited the expression of IL-6 and IL-2 *in vitro*. Immunofluorescence was used to show distributions of IL-2 (red, **E–H**) and GFAP (green, **A–D**) with the merge pictures shown in **(D, H, L, Y)**. Double labeled immunofluorescence showed the expression of GFAP (green, **M–P**) and IL-6 (red, **Q–T**), and the co-localization was shown in **(U–W)** and **(X, Z)**. with a sample size of N=4 and significance level of ***P<0.005, and ****P<0.001. Scale bars for **(A–X)** were set at 50 μm.

mechanism in stroke. Treg cell depletion reduced these structural alterations, while IL-2 administration enhanced them. Secondly, depletion of Treg cells only resulted in impairments in white matter (WM) integrity and behavioral performance during the late stages of recovery, as opposed to the early stage after stroke. Similarly, the IL-2-mediated increase in Treg cells led to behavioral improvements solely in the late phase of stroke (22, 23). Additionally, delaying Treg cell depletion until 5 days after transient middle cerebral artery occlusion (tMCAO) worsened WM injury following stroke. Our study found that 14 days after cerebral infarction, there was activation of astrocytes in the brain, accompanied by an increased secretion of IL-2 and IL-6. When

10.3389/fimmu.2023.1255316

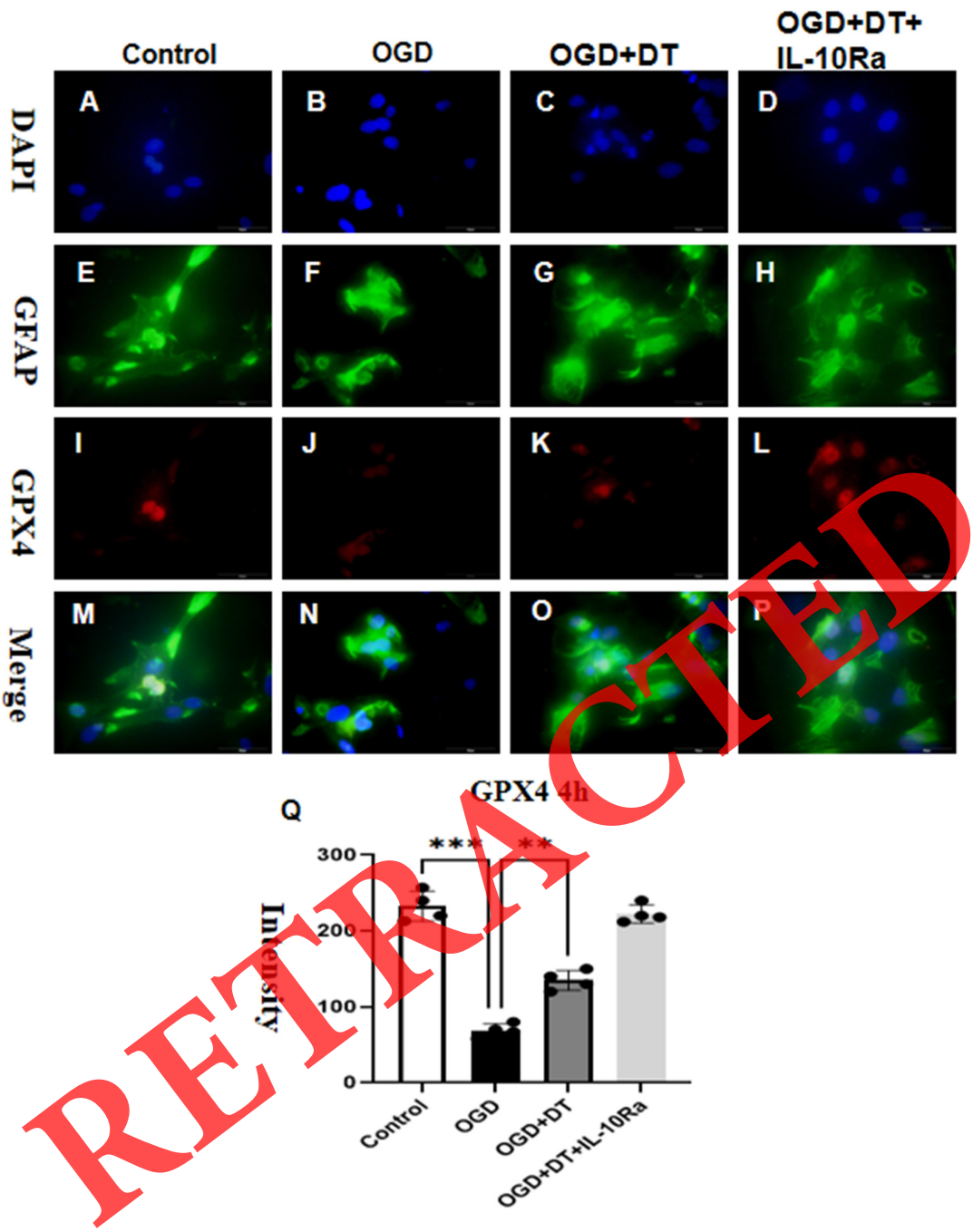

FIGURE 8
DT promoted astrocytes ferroptosis by inhibiting the IL-10/GPX4 pathway. The fluorescence intensities of GPX4 was measured for each group *in vitro* 4h after OGD treatment, as shown in **(A–T)**. OGD caused a significant decrease in GPX4 protein expression levels **(E–H)**. Conversely, treatment with DT decreased GPX4 expression in astrocytes **(I–L)**. Furthermore, adding IL-10Ra, an IL-10 inhibitor, increased the effect of OGD **(M–Q)**, with N = 4 and **P<0.01, ***P<0.005 indicating statistical significance. **(A–P)** features a scale bar of 50 μm.

Tregs were knocked out, the expression of IL-2 and IL-6 was higher than in the cerebral infarction group.

Ferroptosis is a form of cell death that is regulated by metabolism. It is characterized by the accumulation of iron-dependent lipid hydroperoxides to lethal levels (7, 8). Various inducers can trigger ferroptosis. RSL3, for example, acts as a GPX4 inhibitor, increasing lipid peroxidation. Furthermore, inhibitors of the system xc-, such as erastin and its analogs, induce ferroptosis by impairing cystine import and depleting intracellular GSH. In addition to ferroptosis inducers, there have been several pharmacological inhibitors discovered. Agents that inhibit lipid peroxidation, such as Ferrostatin-1 (Fer-1) and liproxstatins, are capable of suppressing ferroptosis (24–27). Glutathione peroxidases (GPXs) are a group of antioxidant enzymes commonly expressed in various human tissues to detoxify peroxides (28). The GPX enzyme family consists of eight members. GPX4 is currently the only known enzyme capable of directly

eliminating lipid peroxides. It converts harmful lipid peroxides into harmless substances and ultimately disrupts the process of lipid peroxidation, thereby inhibiting cell ferroptosis (29, 30). Inhibiting GPX4 activity leads to the accumulation of lipid peroxides, which serves as an indicator of ferroptosis in cells (31). Our investigation discovered that the administration of DT significantly decreased GPX4 expression levels in mice with MCAO. These findings suggest that DT promotes ferroptosis in cerebral infarction, although the specific mechanism remains unclear.

FSP1, previously known as an endogenous inhibitor of ferroptosis (32), suppresses the expression of coenzyme Q10, thereby promoting the production of lipophilic free radicals. According to Santoro (33), RTA can counteract the accumulation of lipid peroxides, effectively alleviating ferroptosis. It has been reported that FSP1 can assist cancer cells in resisting ferroptosis and support the growth of lung cancer cells even in the absence of GPX4 activity (34). Therefore, FSP1 serves as a vital target for drug therapy in cancer management. Researchers have identified that iFSP1 can significantly increase the susceptibility of tumor cells to ferroptosis and also influence ubiquinol metabolism (35), which may impede the onset of ferroptosis in cells. Our investigation revealed that treatment with Fer-1 substantially elevated the levels of FSP1 expression in mice with MCAO.

Tissue-resident Tregs, naturally present in various organs or accumulating in damaged tissues, have been the subject of extensive research in recent years. It has been demonstrated that tissue Tregs undergo gradual maturation in lymph nodes and subsequently acquire their distinct characteristics within tissues. However, the environmental factors necessary for tissue Treg development have yet to be elucidated. To the best of our knowledge, no *in vitro* methods for inducing tissue Tregs have been reported thus far. Through the utilization of a mouse model of cerebral infarction, we demonstrated the activation and proliferation of brain Tregs, both in cervical lymph nodes and the brain, mediated by IL-2 (36–41).

Our findings are consistent with previous research that has shown an increase in IL-6 release and a decrease in the anti-inflammatory cytokine IL-10 in response to MCAO stimulation. There is significant evidence linking multiple regulators with cell death. Our study demonstrated that DT prevents the formation of astrocytes in mice with MCAO. To examine whether DT can impact astrocytes by managing ferroptosis, we employed IL-10Ra *in vitro*.

5 Conclusion

MCAO stimulation impairs inflammatory pathways, reducing the effectiveness of astrocytes response against infections. Tregs priming leads to upregulation of protein expression associated with the IL-10 pathway, causing disrupted cellular homeostasis in cases of MCAO and highlighting the significant role of this mechanism in Tregs. Our research provides that tregs depletion aggravates activation of astrocytes by modulating IL-10/GXP4 following cerebral infarction and provides new therapeutic directions for the prevention and treatment of MCAO.

Data availability statement

The original contributions presented in the study are included in the article/Supplementary Material. Further inquiries can be directed to the corresponding authors.

Ethics statement

The animal studies were approved by Clinical Ethical Committee of Xinhua Hospital Affiliated with Shanghai Jiao Tong University School of Medicine. (No. (2022) 189). The studies were conducted in accordance with the local legislation and institutional requirements. Written informed consent was obtained from the owners for the participation of their animals in this study.

Author contributions

SW: Writing – original draft, Writing – review & editing. YS: Methodology, Writing – original draft. YZ: Data curation, Writing – original draft. FY: Software, Writing – original draft. JM: Resources, Supervision, Writing – original draft, Writing – review & editing. MM: Resources, Supervision, Writing – original draft, Writing – review & editing.

Funding

Emergency Specialty - Department of Emergency Medicine (YXMZK005); General Discipline at TongRen Hospital (tr2023xk36).

Conflict of interest

The authors declare that the research was conducted in the absence of any commercial or financial relationships that could be construed as a potential conflict of interest.

The reviewer DX declared a shared parent affiliation with the authors to the handling editor at the time of the review.

Publisher's note

Supplementary material

The Supplementary Material for this article can be found online at: https://www.frontiersin.org/articles/10.3389/fimmu.2023.1255316/full#supplementary-material

References

1. Frantz C, Auffray C, Avouac J, Allanore Y. Regulatory T cells in systemic sclerosis. *Front Immunol* (2018) 9:2356. doi: 10.3389/fimmu.2018.02356

2. Petersen J, Kooy-Winkelaar Y, Loh KL, Tran M, van Bergen J, Koning F, et al. Diverse T cell receptor gene usage in HLA-DQ8-associated celiac disease converges into a consensus binding solution. *Structure* (2016) 24:1643–57. doi: 10.1016/j.str.2016.07.010

3. Guo X, Zhang Y, Zheng L, Zheng C, Song J, Zhang Q, et al. Global characterization of T cells in non-small-cell lung cancer by single-cell sequencing. *Nat Med* (2018) 24(7):978–85. doi: 10.1038/s41591-018-0045-3

4. Guo W, Zhang C, Wang X, Dou D, Chen D, Li J. Resolving the difference between left-sided and right-sided colorectal cancer by single-cell sequencing. *JCI Insight* (2022) 7:e152616. doi: 10.1172/jci.insight.152616

5. Akimova T, Zhang T, Christensen LM, Wang Z, Han R, Negorev D, et al. Obesity-related IL-18 impairs T-regulatory cell function and promotes lung ischemia-reperfusion injury. *Am J Respir Crit Care Med* (2021) 204:1060–74. doi: 10.1164/rccm.202012-4306OC

6. Xu J, Li X, Yuan Q, Wang C, Xu L, Wei X, et al. The semaphorin 4A-neuropilin 1 axis alleviates kidney ischemia reperfusion injury by promoting the stability and function of regulatory T cells. *Kidney Int* (2021) 100:1268–81. doi: 10.1016/j.kint.2021.08.023

7. Ito M, Komai K, Nakamura T, Srirat T, Yoshimura A. Tissue regulatory T cells and neural repair. *Int Immunol* (2019) 31:361–9. doi: 10.1093/intimm/dxz031

8. Hamanaka G, Ohtomo R, Takase H, Lok J, Arai K. White-matter repair: Interaction between oligodendrocytes and the neurovascular unit. *Brain Circ* (2018) J4:118–23. doi: 10.4103/bc.bc_15_18

9. Azad TD, Veeravagu A, Steinberg GK. Neurorestoration after stroke. *Neurosurg Focus* (2016) 40:E2. doi: 10.3171/2016.2.FOCUS15637

10. Dixon SJ, Lemberg KM, Lamprecht MR, Skouta R, Zaitsev EM, Gleason CE, et al. Ferroptosis: an iron-dependent form of nonapoptotic cell death. *Cell* (2012) 149:1060–72. doi: 10.1016/j.cell.2012.03.042

11. Yu Y, Yan Y, Niu F, Wang Y, Chen X, Su G, et al. Ferroptosis: a cell death connecting oxidative stress, inflammation and cardiovascular diseases. *Cell Death Discovery* (2021) 7:193. doi: 10.1038/s41420-021-00579-w

12. Zou M, Wang K, Zhao J, Lu H, Yang H, Huang M, et al. DegS protease regulates the motility, chemotaxis, and colonization of Vibrio cholerae. *Front Microbiol* (2023) 14:1159986. doi: 10.3389/fmicb.2023.1159986

13. Powers RK, Goodspeed A, Pielke-Lombardo H, Tan AC, Costello JC. GSEA-InContext: identifying novel and common patterns in expression experiments. *Bioinformatics* (2018) 34:i555–64. doi: 10.1093/bioinformatics/bty271

14. The Gene Ontology Consortium. The Gene Ontology Resource: 20 years and still GOing strong. *Nucleic Acids Res* (2019) 47(D1):D330–8. doi: 10.1093/nar/gky1055

15. Kanehisa M, Furumichi M, Tanabe M, Sato Y, Morishima K. KEGG: new perspectives on genomes, pathways, diseases and drugs. *Nucleic Acids Res* (2017) 45:D353–61. doi: 10.1093/nar/gkw1092

16. Martino E, Chiarugi S, Margheriti F, Garau G. Mappings structure and modulation of PPI. *Front Chem* (2021) 9:718405. doi: 10.3389/fchem.2021.718405

17. McBride DW, Zhang JH. Precision stroke animal models: the permanent MCAO model should be the primary model, not transient MCAO. *Transl Stroke Res* (2017) 17. doi: 10.1007/s12975-017-0554-2

18. Im K, Mareninov S, Diaz MFP, Yong WH. An introduction to performing immunofluorescence staining. *Methods Mol Biol* (2019) 1897:299–311. doi: 10.1007/978-1-4939-8935-5_26

19. Kidani Y, Nogami W, Yasumizu Y, Kawashima A, Tanaka A, Sonoda Y, et al. CCR8-targeted specific depletion of clonally expanded Treg cells in tumor tissues evokes potent tumor immunity with long-lasting memory. *Proc Natl Acad Sci U.S.A.* (2022) 119:e2114282119. doi: 10.1073/pnas.2114282119

20. Zhang L, Wang Y, Pan RL, Li Y, Hu YQ, Xv H, et al. Neuritin attenuates oxygen-glucose deprivation/reoxygenation (OGD/R)-induced neuronal injury by promoting autophagic flux. *Exp Cell Res* (2021) 407(2):112832. doi: 10.1016/j.yexcr.2021.112832

21. Mitteer DR, Greer BD. Using graphPad prism's heat maps for efficient, fine-grained analyses of single-case data. *Behav Anal Pract* (2022) 15(2):505–14. doi: 10.1007/s40617-021-00664-7

22. Zhu H, Hu S, Li Y, Sun Y, Xiong X, Hu X, et al. Interleukins and ischemic stroke. *Front Immunol* (2022) 13:828447. doi: 10.3389/fimmu.2022.828447

23. Hernandez R, Põder J, LaPorte KM, Malek TR. Engineering IL-2 for immunotherapy of autoimmunity and cancer. *Nat Rev Immunol* (2022) 22:614–28. doi: 10.1038/s41577-022-00680-w

24. Wu X, Li Y, Zhang S, Zhou X. Ferroptosis as a novel therapeutic target for cardiovascular disease. *Theranostics* (2021) 11(7):3052–9. doi: 10.7150/thno.54113

25. Liu P, Feng Y, Li H, Chen X, Wang G, Xu S, et al. Ferrostatin-1 alleviates lipopolysaccharide-induced acute lung injury *via* inhibiting ferroptosis. *Cell Mol Biol Lett* (2020) 25:10. doi: 10.1186/s11658-020-00205-0

26. Gao W, Wang X, Zhou Y, Wang X, Yu Y. Autophagy, ferroptosis, pyroptosis, and necroptosis in tumor immunotherapy. *Signal Transduct Target Ther* (2022) 7 (1):196. doi: 10.1038/s41392-022-01046-3

27. Sun Y, Chen P, Zhai B, Zhang M, Xiang Y, Fang J, et al. The emerging role of ferroptosis in inflammation. *BioMed Pharmacother* (2020) 127:110108. doi: 10.1016/j.biopha.2020.110108

28. Bersuker K, Hendricks JM, Li Z, Magtanong L, Ford B, Tang PH, et al. The CoQ oxidoreductase FSP1 acts parallel to GPX4 to inhibit ferroptosis. *Nature* (2019) 7784:688–92. doi: 10.1038/s41586-019-1705-2

29. Jia M, Qin D, Zhao C, Chai L, Yu Z, Wang W, et al. Redox homeostasis maintained by GPX4 facilitates STING activation. *Nat Immunol* (2020) 21(7):727–35. doi: 10.1038/s41590-020-0699-0

30. Miao Y, Chen Y, Xue F, Liu K, Zhu B, Gao J, et al. Contribution of ferroptosis and GPX4's dual functions to osteoarthritis progression. *EBioMedicine* (2022) 76:103847. doi: 10.1016/j.ebiom.2022.103847

31. Wang Y, Zheng L, Shang W, Yang Z, Li T, Liu F, et al. Wnt/beta-catenin signaling confers ferroptosis resistance by targeting GPX4 in gastric cancer. *Cell Death Differ* (2022) 11:2190–202. doi: 10.1038/s41418-022-01008-w

32. Doll S, Freitas FP, Shah R, Aldrovandi M, da Silva MC, Ingold I, et al. FSP1 is a glutathione-independent ferroptosis suppressor. *Nature* (2019) 575(7784):693–8. doi: 10.1038/s41586-019-1707-0

33. Koppula P, Lei G, Zhang Y, Yan Y, Mao C, Kondiparthi L, et al. A targetable CoQ-FSP1 axis drives ferroptosis- and radiation-resistance in KEAP1 inactive lung cancers. *Nat Commun* (2022) 13(1):2206. doi: 10.1038/s41467-022-29905-1

34. Yang M, Tsui MG, Tsang JKW, Goit RK, Yao KM, So KF, et al. Involvement of FSP1-CoQ10-NADH and GSH-GPx-4 pathways in retinal pigment epithelium ferroptosis. *Cell Death Dis* (2022) 13:468. doi: 10.1038/s41419-022-04924-4

35. Müller F, Lim JKM, Bebber CM, Seidel E, Tishina S, Dahlhaus A, et al. Elevated FSP1 protects KRAS-mutated cells from ferroptosis during tumor initiation. *Cell Death Differ* (2023) 30(2):442–56. doi: 10.1038/s41418-022-01096-8

36. Miragaia RJ, Gomes T, Chomka A, Jardine L, Riedel A, Hegazy AN, et al. Single-cell transcriptomics of regulatory T cells reveals trajectories of tissue adaptation. *Immunity* (2019) 50:493–504.e7. doi: 10.1016/j.immuni.2019.01.001

37. DiSpirito JR, Zemmour D, Ramanan D, Cho J, Zilionis R, Klein AM, et al. Molecular diversification of regulatory T cells in nonlymphoid tissues. *Sci Immunol* (2018) 3:eaat5861. doi: 10.1126/sciimmunol.aat5861

38. Li C, DiSpirito JR, Zemmour D, Spallanzani RG, Kuswanto W, Benoist C, et al. TCR transgenic mice reveal stepwise, multi-site acquisition of the distinctive fat-treg phenotype. *Cell* (2018) 174:285–299.e12. doi: 10.1016/j.cell.2018.05.004

39. Overwijk WW, Tagliaferri MA, Zalevsky J. Engineering IL-2 to give new life to T cell immunotherapy. *Annu Rev Med* (2021) 72:281–311. doi: 10.1146/annurev-med-073118-011031

40. Jiang X, Stockwell BR, Conrad M. Ferroptosis: mechanisms, biology and role in disease. *Nat Rev Mol Cell Biol* (2021) 22:266–82. doi: 10.1038/s41580-020-00324-8

41. Li J, Cao F, Yin HL, Huang ZJ, Lin ZT, Mao N, et al. Ferroptosis: past, present and future. *Cell Death Dis* (2020) 11:88. doi: 10.1038/s41419-020-2298-2